How Should Snowball Earth Deglaciation Start

Jiacheng Wu[1], Yonggang Liu[1], Zhouqiao Zhao[1]

[1] Department of Atmospheric and Oceanic Sciences, School of Physics, Peking University, Beijing, 100871, China

Contact information of the corresponding author

Email: ygliu@pku.edu.cn

Phone: (+86)-10-62769125

Fax: (+86)-10-62751094

Abstract

Formation of melt ponds is pervasive on sea ice and ice shelves prior to their disintegration. Such process should be critical for the deglaciation of a snowball Earth but has never been considered in previous studies. Here we develop a module to explicitly track the initiation, growth and refreezing of melt ponds on ice. Incorporation of the module into a climate model indicates that it provides a strong positive feedback to the climate, and previous studies seriously overestimated the threshold CO_2 at which a snowball Earth deglaciates. At CO_2 level of 0.1 bar and without the melt pond effect, the annual mean equatorial surface temperature is only -7.7 °C, far from deglaciating. However, this temperature increases to 6.1 °C in a few tens of years once melt pond effect is turned on. The results also demonstrate unambiguously that the deglaciation of snowball Earth should start from the equator, although seasonal melt ponds may appear first in the subtropical regions.

Key words: Snowball Earth; Deglaciation, Neoproterozoic, Snow aging; Melt pond

1. Introduction

Once Earth enters a snowball Earth state (Hoffman et al., 2017a; Hoffman et al., 2017b; e.g. Hoffman et al., 1998), it is very difficult to recover because the whole globe will be covered by highly reflective snow and ice. Early estimates using energy balance models (EBMs) showed that 0.16 - 0.29 bar of CO_2 was required to deglaciate the Neoproterozoic (1000 – 541 Ma) snowball Earth (Caldeira & Kasting, 1992; Tajika, 2003). Later studies using general circulation models (GCMs) obtained similar results, i.e., greater than 0.1 bar of CO_2 was required to initiate the deglaciation (Hu et al., 2011; Le Hir et al., 2007; Pierrehumbert, 2004). To facilitate the deglaciation, deposition of volcanic dust and other terrestrial dust have been invoked to lower the surface albedo (e.g. Li & Pierrehumbert, 2011b) or planetary albedo (Abbot & Halevy, 2010). Voluminous dust in the atmosphere or in the ice could lower the threshold CO_2 level for snowball Earth deglaciation to a range of 0.01 – 0.1 bar (Abbot & Halevy, 2010; Abbot & Pierrehumbert, 2010; Le Hir et al., 2010).

The start of deglaciation is usually judged by whether the maximum monthly mean (Hu et al., 2011; Pierrehumbert, 2004) or annual mean surface temperatures (Abbot et al., 2013b; Le Hir et al., 2010) approach 0 °C. The former first appears in the subtropical regions while the latter appears in the equatorial region. This criterion is quite crude because melt ponds start to form on ice whenever the instant surface temperature is near 0 °C (Polashenski et al., 2012), i.e. at monthly mean surface temperatures much lower than 0 °C since there will be strong diurnal and daily temperature fluctuations. Melt ponds have two effects on snowball Earth climate. The first is that it reduces the surface albedo and provides a positive feedback to the warming induced by increasing CO_2. It

may thus allow deglaciation to start at a lower CO_2 than when the melt pond is not considered. The second effect is that the melt ponds, if prevalent on the ice surface, may cause thick floating sea ice to break and calve. This has been observed during the calving of ice shelf Larson B in Antarctic Peninsula (e.g. Banwell et al., 2013). Therefore, finding when and where extensive melt ponds appear on ice surface may tell us directly at what CO_2 concentration the deglaciation will start and whether the deglaciation starts from subtropical or equatorial region.

Melt ponds on ice can be considered in two distinctly different ways in climate models. The first is to simply parameterize its albedo effect by assuming a linear reduction of albedo with surface temperature. This is normal practice in sea-ice modeling in many climate models but they all differ in when the ice albedo starts to decrease and by how much (see Fig. 1 of Hu et al., 2011),. For example, in some models the sea-ice albedo starts to decrease when the instant surface temperature is -10 °C, while others start at -1 °C, and some decrease the sea-ice albedo by as much as 0.25 while others may decrease by only 0.07 as temperature increases to 0 °C. Moreover, such parameterization does not track the evolution of thickness of melt ponds and thus does not allow the melt ponds to persist through diurnal or seasonal cycles. A more sophisticated way of modeling the effect of melt ponds is to explicitly calculate their depth and their influence on albedo based on the depth. Our purpose herein is to develop such a scheme in the climate model and test how they will affect the deglaciation of a snowball Earth.

Melt ponds form on snow too, especially for thin snow on ice because melt water cannot percolate downward easily but accumulate on the surface; when undulations of snow thickness exist, as they normally do, melt ponds tend to form around snow dunes (Petrich et al., 2012; Webster et al., 2018). We do not intend to consider such detailed processes here but pay much attention to the effect of snow aging instead. The reason for this is that we found that the snow depth in a snowball Earth simulated by the climate model was always thick (~ 1 m water equivalent) if the effect of snow aging was ignored; melt water of snow, if there was any, would likely drip down into deeper snow rather than accumulate at the surface. If snow aging was considered, snow thickness on ice has two contrasting regimes; it was negligible within the equatorial and subtropical latitudinal bands but very thick (> 0.6 m) in other regions (see Fig. 4d below). Therefore, only melt ponds on ice need to be considered. Snow aging is an important process in reducing snow albedo (Le Hir et al., 2010, and reference there) and thus snow thickness, the latter of which pre-conditions the appearance of melt ponds on ice.

The effect of snow aging was unintentionally ignored in the simulations of Hu et al. (2011). The model they used was an atmospheric general circulation model (AGCM), CAM3, coupled to a land surface module, CLM3. Snow aging and its albedo effect are considered in CLM3 (Oleson et al., 2004), but not in the thermodynamic sea-ice module within CAM3 (Collins et al., 2004). Hu et al. (2011) prescribed thick sea ice over the ocean rather than treating sea ice as continental glaciers (e.g. Abbot et al., 2013b), so they did have the effect of melt ponds (parameterized) on the albedo of both snow and ice but not the effect of snow aging. Without snow aging, their simulations gave very cold climate and melt ponds most likely did not take effect either. Moreover, their simulations

were carried out for only a few tens of years, far from enough for initial deep snow (1 m water equivalent) on ice to sublimate and expose the ice below (Liu et al., 2020). Therefore, they found that the deglaciation of a snowball Earth could not be initiated even when the atmospheric CO_2 level (pCO_2) was as high as 0.3 bar. We will show herein that the threshold pCO_2 is much lower than 0.3 bar once the effect of snow aging is turned on in the same model. Moreover, we show that seasonal melt ponds develop first at subtropical regions but perennial and deep melt ponds appear first at the equator if melt ponds are simulated explicitly.

The rest of the paper is organized as follows. A brief description of the model used is provided in section 2.1, the formulation for melt ponds on ice is described in section 2.2, the experiments carried out in this study are summarized in section 2.3. The results are presented in section 3, and the implication of these results to snowball Earth deglaciation is discussed in section 4. Finally, conclusions are reached in section 5.

2. Model and experimental design

2.1 Climate Model and snow aging

The Community Atmosphere Model version 3 (CAM3) and Community Land Model version 3 (CLM3) used in this study were both developed by the National Center for Atmospheric Research. CAM3 solves the primitive equations in a generalized terrain-following vertical coordinate. The equations are solved with a spectral dynamic core with triangular truncation at wavenumber 31 (T31), which is equivalent to a horizontal spatial resolution of ~3.75° × 3.75°. The model has 26 vertical levels from the surface to approximately 2 hPa (Collins et al., 2004). The module CLM3 deals with vegetation,

121 wetland and lakes, glaciers, hydrological cycle on land, and thermodynamics of soil and
122 snow (Oleson et al., 2004). Its horizontal resolution is the same as CAM3. The glaciers
123 are prescribed in the module and thus cannot evolve. The albedo of glacier is 0.6 and 0.4
124 for the visible and near infrared wavebands, respectively, independent of the solar zenith
125 angle. This albedo is typical for glacial ice (Paterson, 1994), and is similar to the sea-ice
126 albedo used in Hu et al. (2011). For all simulations herein, sea ice is considered as glacier
127 since it is very thick and moves slowly like glaciers (Ashkenazy et al., 2014).

128 The albedo of snow-covered ground is dependent on the thickness of snow and the solar
129 zenith angle, and is distinguished for direct and diffuse beam radiation (Oleson et al.,
130 2004). Here we only describe how snow age is determined and how it affects snow
131 albedo in CLM3. Newly fallen snow has an age of zero, and its non-dimensional age
132 increases with time as:

133 $$\tau_{sno}(t+\Delta t) = (1 - 0.1\Delta W_{sno})[\tau_{sno}(t) + (r_v(T) + r_d)r_0\Delta t] \quad (1)$$

134 where r_0 is 1×10^{-6} s^{-1}, Δt is the model time step, r_v takes into account of the effect of
135 grain growth due to vapor diffusion and is dependent on snow temperature, r_d considers
136 the effect of dirt, and ΔW_{sno} is the change in mass of snow (kg m^{-2}) relative to the last
137 time step. The terms in the first bracket on the RHS means that if 10 kg m^{-2} of new snow
138 falls on the surface of unit area (1 m^2), the snow age is restored to 0. The detailed form of
139 r_v is not laid out here since we have no good reason to change it herein but its variation
140 with temperature is shown in Fig. 1a. The value of r_d is taken to be a constant, 0.3, by
141 default in the model. However, since the amount of dust is uncertain during a snowball
142 Earth, a few sensitivity tests will be carried out to test its influence on the snowball Earth

climate. In these tests, r_d is reduced to 0.2, 0.1 and 0.03, respectively, and its influence on snow age is shown in Fig. 1b. The non-dimensional snow age is reduced by ~14 percent when r_d is reduced from 0.3 to 0.03. This change seems to be small but have significant influence on the simulated surface temperature in a snowball Earth.

Snow albedo decreases with the non-dimensional snow age according to

$$\alpha_{sno,\Lambda} = \left[1 - C_\Lambda \left(1 - \frac{1}{1+\tau_{sno}}\right)\right] \alpha_{sno,\Lambda,0} \quad (2)$$

where the albedo of new snow $\alpha_{sno,\Lambda,0}$ is 0.95 and 0.65 for the visible and near infrared wavebands and the empirical constant C_Λ is 0.2 and 0.5 for the two wavebands, respectively. The albedo of oldest snow is then 0.76 and 0.325 for the two wavebands, respectively (Fig. 1c). The full spectrum average (with a partition of radiative flux between the visible and near-infrared wavebands being 53% versus 47%) is thus 0.56, still higher than that for the glacier. In order to prevent melting of ice sheets over present-day Greenland and Antarctica, snow age has been hard coded to 0 in CLM3 whenever snow depth is greater than 800 mm. Such constraint is removed herein because we think that it will greatly overestimate the albedo of snow especially when precipitation rate is very low such as in a snowball Earth.

2.2 Melt pond formulation

Deglaciation of a snowball Earth must start with formation of melt ponds on the surface of thick sea-ice sheet. This process is not considered for the glaciers in CLM3, so we have to implement one by ourselves. In reality, melt ponds may consist of multiple layers of water and ice interleaved with each other due to seasonal, daily or diurnal melting and

freezing (Hunke et al., 2013). Here we simplify the process by considering only three possible stages of the melt ponds: no melt pond, melt pond without and with one layer of ice lid (Fig. 2). That is, we do not consider the formation of melt pond on ice lid and new layer of ice lid on this second layer of melt pond.

The vertical temperature profiles in the ice, melt pond and ice lid are also simplified (Fig. 2). Right before melt ponds start to form, e.g., near noon of a certain day in summer, the temperature of near surface ice is assumed to be constant and at freezing point ($T_f \equiv 0$ °C) of pure water (stage I in Fig. 2). This assumption is not bad since the heat of fusion of water is more than 80 times the heat required to raise the temperature of the same amount of ice by 1 °C. After melt pond forms, the temperature profile is assumed to be linearly increasing from T_f at the bottom to the large scale (i.e., model-grid scale) ground surface temperature T_g calculated by the model. Such assumption is probably not so valid when the water temperature is below 4 °C as pure water is densest at 4 °C; vertical convection will tend to reduce the temperature gradient so that the temperature profile may look more like the dotted curve in stage II of Fig. 2 (Bogorodsky et al., 2006; Roeckner et al., 2012; Scharien et al., 2014). This temperature profile is mainly used to calculate how much energy is being transferred to the bottom of pond and melting ice there. When the surface cools at night, an ice lid may form at the top of melt pond. In this stage, the temperature of water becomes T_f and the temperature within the lid is assumed to increase or decrease linearly from T_f at the bottom to surface temperature T_g at the top. This latter assumption of linearity is also a simplification of the reality because the interior temperature of the ice may not respond to surface temperature quickly, and it

186 could be higher than the surface temperature due to penetration of sunlight into the ice
187 interior.

188 The change of ice lid and pond water is governed by the Stefan condition at the phase
189 boundaries (Hunke et al., 2013)

190 $$\rho_w L \frac{\partial h_w}{\partial t} \approx -k_w \frac{\partial T_w}{\partial z} \quad (3)$$

191 $$\rho_i L \frac{\partial h_l}{\partial t} \approx k_i \frac{\partial T_l}{\partial z} \quad (4)$$

192 where L is the latent heat of fusion of pure ice per unit volume, ρ_w and ρ_i are densities of
193 ice and water, h_w and h_l are thicknesses of the pond water and ice lid, k_w and k_i are
194 thermal conductivities of the meltwater and ice lid, and T_w and T_l are temperatures near
195 the phase boundary of pond water and ice lid, respectively.

196 Because linear temperature profile has been assumed for the whole pond water, the
197 magnitude of right-hand side (RHS) of equ. (3) may be either underestimated or
198 overestimated. When pond water is thin, ice can melt by absorbing sunlight directly;
199 when pond water is a few tens of centimeter thick, the temperature gradient may be
200 strengthened near the bottom as shown in Fig. 2 (middle); when pond water is a few
201 meters thick, the temperature gradient may be strengthened again near the bottom
202 because the temperature of water near the surface is well mixed beneath which a sharp
203 thermocline forms as often observed in lakes (Axenrot et al., 2009; Schwarz et al., 2016).
204 For these situations that are of the greatest relevance herein, the temperature gradient in
205 the RHS of equ. (3) is underestimated. Only when pond water is very thick (>> 10 m), the
206 temperature gradient may be overestimated because water temperature tends be near

207 constant below the thermocline in lakes (e.g. Stepanenko et al., 2010). Influence of the
208 uncertainty in the temperature gradient of equ. (3) on the melt ponds and snowball Earth
209 climate is tested in section 4.1.

210 The magnitude of right-hand side (RHS) of equ. (4) is likely always overestimated; when
211 ice lid is thin, sunlight can penetrate through the lid and increase its bottom temperature,
212 while when it is thick, interior temperature of the lid responds slowly to the surface
213 temperature and creates a relatively small temperature gradient near the bottom.
214 Therefore, both equs. (3) and (4) are expected to underestimate the growth of pond water
215 when the depth of water is not very thick (e.g. <10 m). Note that ice lid has two phase
216 boundaries. When surface temperature is high enough, melting always starts at the
217 surface of the ice lid and melt water produced is assumed to leak into the melt pond
218 beneath immediately. Nothing happens at the bottom of the lid. Also, no melting will start
219 at the bottom of melt pond until the lid is completely melt away.

220 The ice surface is initialized to stage I at the beginning of a run. Stage II starts to appear
221 when the grid-scale surface temperature is greater than 0 °C. When temperature decreases
222 to below 0 °C, stage II will transform to stage III but not necessarily all the way to stage I
223 before temperature starts to rise again. The thicknesses of pond water and ice lid are
224 tracked at every time step of the model run. Unlike sea ice of present day, which is thin
225 and pond water may leak into the ocean beneath easily through leads (Eicken et al., 2002;
226 Richter-Menge et al., 2001), the sea ice is so thick during a snowball Earth that we do not
227 need to worry about the loss of pond water.

The surface albedo of infinitely thick ice is affected by the presence of pond water (Taylor & Feltham, 2004),

$$\alpha_p = R_0 + \frac{(1-R_0)^2 s_{ice} e^{-(\tau+2\kappa)h_w}}{1-R_0 s_{ice} e^{-(\tau+2\kappa)h_w}}, s_{ice} = \frac{\alpha_i - R_0}{1-2R_0+\alpha_i R_0} \quad (5)$$

where α_i is the albedo of infinitely thick ice (the albedo of glacier) and α_p is the albedo when there is melt pond of h_w thick. $R_0 = 0.05$ is the Fresnel reflection coefficient of water, $\tau = 3.55$ is the fitting parameter, $\kappa = 0.025$ m^{-1} is the extinction coefficient of water. When ice lid of h_l is present, the surface albedo becomes (Briegleb et al., 2004)

$$\alpha_e = f_h \cdot \alpha_i + (1 - f_h) \cdot \alpha_p, \ f_h = min\left(\frac{arctan(c_{fh} \cdot h_l)}{arctan(c_{fh} \cdot h_{l_c})}, 1.0\right) \quad (6)$$

where $c_{fh} = 4, h_{l_c} = 0.5$ m are empirical parameters, *arctan* is the inverse tangent function. When the thickness of ice lid is greater than 0.5 m, the effective surface albedo is equal to the albedo of glacier.

To get the surface albedo of a grid cell of the climate model, the areal fraction of melt pond within the grid cell is needed. We assume that the temperature at any point (e.g., with an area of 1 m^2) is random due to turbulence in the atmosphere and fluctuates around the grid cell temperature according to a normal distribution, with a standard deviation σ = 1 °C. Then the fraction of grid cell that has temperature greater than T_f is

$$C = 1 - \Phi\left(\frac{T_f - T_g}{\sigma}\right) \quad (7)$$

where Φ is cumulative distribution function of the standard normal distribution (Ross, 2010). Note that this fraction is greater than zero even when T_g is 20 °C below T_f, but is

247 negligible. We calculate the formation of melt pond only when T_g range from T_f-2σ and
248 T_f+2σ. The average temperature over this part of the grid cell is

249 $$\bar{T}_{g_{melt}} = T_g + \frac{\sigma}{C\sqrt{2\pi}} e^{-\frac{(T_f - T_g)^2}{2\sigma^2}} \quad (8)$$

250 This temperature is used to calculate the thickness of meltwater within each grid cell. The
251 calculated thicknesses are then multiplied by factor C to get grid-mean thicknesses, which
252 is used to calculate the grid-mean surface albedo. The value of σ is uncertain but 1 °C
253 should be an underestimate; without considering the air turbulence, the temperature
254 difference between the southern and northern boundaries of a grid cell can be greater than
255 1 °C even in the low-latitude region due to the coarse resolution of the model. Increasing
256 of σ enhances formation of melt pond (see section 4.1).

257 **2.3 Experimental design**

258 In all experiments carried out herein, continents and oceans are not distinguished since
259 both of them are covered by thick ice. The surface of the whole globe is treated as
260 continental glacier, similar to the setup in Abbot et al. (2013b). The surface topography is
261 ignored, to be consistent with the model setup in Hu et al. (2011). The initial snow depth
262 is uniformly 1 m water equivalent. Present-day orbital configuration of the Earth is
263 assumed. The atmospheric concentrations of CH_4, N_2O are all pre-industrial level. CFCs
264 are set to zero. In all experiments carried out here, solar constant is 94% of present-day
265 value and pCO_2 is 0.1 bar.

266 Three sets of experiments are carried out. In the first set of five experiments, the climate
267 impact of snow aging is tested. Effect of melt pond is not considered in this set of

268 experiment. The first experiment (experiment Default) uses the default setting for snow
269 aging calculation, i.e., snow age is fixed to 0 for snow deeper than 800 mm water
270 equivalent, and the other four experiments (rd1 to rd4) removes the restriction. In these
271 four experiments, the snow aging parameter r_d is set to 0.3, 0.2, 0.1 and 0.03,
272 respectively. In the second set of three experiments, the influence of melt pond on climate
273 of snowball Earth near deglaciation is tested. In two of the three experiments (IMP80 and
274 IMP60), implicit melt pond is considered; surface albedo of ice decreases linearly with
275 instant surface temperature to 80% and 60% of the original value when instant
276 temperature becomes 0 °C for the two experiments, respectively (Fig. 3). In the third
277 experiment (EMP_rd1), melt ponds on ice are explicitly modeled using the formulation
278 above. In all three experiments, the snow aging parameter r_d is fixed to 0.3. The third set
279 of four experiments (EMP_rd1, …, EMP_rd4) is the same as the last four experiments of
280 the first set except that here the explicit simulation of melt ponds is implemented. The
281 second and third sets share one experiment, EMP_rd1. All simulations are continued for
282 at least 400 years, and the last 50 years are used for diagnosis of equilibrium climate state.

283 **3. Results**

284 **3.1 Influence of snow aging on the snowball Earth climate**

285 In the default CLM3, snow age is forced to be zero when water equivalent snow depth is
286 greater than 800 mm and initial snow depth on glaciers is 1000 mm. In this case, the
287 surface albedo of the whole globe is high for a snowball Earth unless the climate warms
288 up significantly so that snow depth decreases to below 800 mm. This does not happen
289 even when $p\mathrm{CO_2}$ is 0.1 bar except over three narrow belts around the equator and in

290 subtropical regions where sublimation is strong (Figs. 4a and 4c). If the 800 mm
291 restriction is removed, global snow age increases (Fig. 4f) and surface albedo decreases
292 significantly (Fig. 4b). This causes the surface temperature to increase dramatically
293 (compare Fig. 4h to 4g) and snow coverage to decrease (Fig. 4d). At equilibrium, the
294 global mean surface temperature is -19.9 °C, 31.1 °C higher than in experiment Default.
295 To be consistent with the melt pond formulation in section 2.2, all surface temperature
296 shown herein mean ground surface temperature.

297 The global mean surface temperature is almost the same when r_d is decreased from 0.3 to
298 0.2, and lowered by 1.0 °C and 1.7 °C when r_d is further decreased to 0.1 and 0.03,
299 respectively (Table 1). Although temperature change is small, the time it takes for the
300 climate to reach equilibrium increases significantly when r_d is reduced (Fig. 5). The
301 annual mean temperature around the equator (6°S-6°N) is -7.7 °C and the highest
302 monthly temperature is -3 °C when r_d = 0.3, both below the melting temperature of ice.
303 The highest monthly temperature is found over the subtropical regions and is higher than
304 0 °C (Fig. 6). Clearly, these high temperatures will initiate seasonal melting. Whether that
305 will initiate deglaciation of snowball Earth is hard to judge without considering the effect
306 of melt ponds.

307 **3.2 Influence of melt ponds on snowball Earth climate**

308 Melt ponds indeed have a strong effect on the snowball Earth climate whether they are
309 represented implicitly or explicitly in the model (Fig. 7). The implicit melt ponds start to
310 take effect quickly, within a few years if the more aggressive parameter is used
311 (experiment IMP60; Fig. 7d). In this case, the annual mean surface temperature around

312 the equator rises from about -13.0 °C to the equilibrium temperature of 2.7 °C within 20
313 years, while it takes 50 years to rise to only -7.8 °C when melt ponds are not considered
314 (Fig. 7a). When the less aggressive parameter is used (experiment IMP80), temperature
315 rises more slowly and the equilibrium temperature is -0.5 °C (Fig. 7c). The global mean
316 surface temperature is approximately 13 °C lower than that around the equatorial mean in
317 all these three cases (Fig. 7).

318 When the melt ponds are simulated explicitly (experiment EMP; Fig. 7b), the time it
319 takes for temperature to reach equilibrium is longer than that when implicit melt ponds
320 are used. This is probably not surprising because the melt ponds in this case take time to
321 develop. The final equatorial temperature is 6.1 °C, much higher than those for
322 experiments IMP80 and IMP60. This is not surprising either because explicit melt ponds
323 can grow to large depth (black dashed curve in Fig. 7b), and the surface albedo will be
324 near that of oceans when the pond depth is greater than 1 m. Once the pond is deeper than
325 1 m, further growth in depth will not have any additional climate effect.

326 We could have varied the parameter of the implicit melt pond so that its surface albedo
327 continuously decrease when instant temperature is greater than 0.0 °C, for example, to
328 0.1 when temperature is 5 °C. However, it will be very unrealistic because low albedo
329 (equivalent to deep melt pond) will appear suddenly at noon even though the annual
330 mean temperature is below -20 °C and the monthly mean temperature of the warmest
331 month is -7 °C (not shown). Our explicit melt-pond modeling shows that deep ponds
332 (>10 cm) appear only when monthly mean surface temperature is greater than T_f (Fig. 8).

An example of seasonal evolution of melt pond in the subtropical region (16.7°N) at model year 40 to 41 is shown in Fig. 8. Note that at this time for this specific case, the depth of melt pond is still evolving and has a net increase each year (Fig. 8b), so is the temperature (Fig. 8a). Melt water appears in all months shown in the figure, but is very shallow and appears only in certain hours of a day during the cold months. In the first February of the figure, monthly mean temperature is -10 °C, but the maximum instant temperature can be as high as -0.05 °C, making formation of melt ponds possible. The mean depth of melt ponds for this month is only 0.2 mm. This depth increases rapidly to 9 cm in May, and increases to a maximum of 60 cm in early December (Fig. 8b). Ice lid starts to develop near the end of December but its thickness is negligible. It grows to a maximum of ~60 cm in the second April and then starts to decrease. At this time, there is still melt water beneath the ice lid but the lid is thick enough so that the surface albedo is the same as that of glaciers (Fig. 8c). Near the end of the second June, ice lid disappears and the thickness of pond water recovers to its maximum during the last year. The pond water continues to grow from the second July to early December, becomes deeper than in the last year (Fig. 8b). Please see the video in Supporting Information for the complete evolution of the surface melt ponds.

3.3 Influence of snow-aging parameter when melt ponds are considered

In contrast to results in section 3.1 (e.g. Fig. 5), the snowball Earth climate is much more sensitive to the snow-aging parameter r_d when melt ponds are considered (Fig. 9). Annual mean equatorial temperature is ~6.1 °C for both r_d = 0.3 and 0.2, while it is only -7.7 °C when r_d = 0.1 and 0.03 (Table 1). The latter is almost the same as the temperatures obtained when melt ponds are not considered (experiments rd3 and rd4,

356 Table1). This is a clear indication that the melt ponds are basically not forming when r_d
357 is small. Therefore, existence of dust in the snowball Earth climate is very important to
358 snow aging and its deglaciation.

359 **4. Discussion**

360 **4.1 Further sensitivity test of the explicit melt pond model**

361 In section 2.2, the surface temperature is assumed to fluctuate within a grid cell which has
362 a size of 3.75°×3.75°, and the standard deviation (σ in equ. (7)) of the fluctuation is
363 assumed to be 1 °C. Although we have argued that 1 °C is small compared to the
364 temperature change between the southern and northern boundaries of the grid cell, it is
365 helpful to test how sensitive the results are to the value of this parameter. The results are
366 shown in Fig. 10a. It can be seen that the equilibrium equatorial temperature is insensitive
367 to the change of σ within the range 0 °C – 2.0 °C. When σ is lowered to 0.25 °C,
368 development of melt ponds nearly halts and the equatorial temperature is similar to when
369 melt ponds are not considered (experiment rd1; Table 1). These tests show that as long as
370 σ is large enough so that some formation of melt ponds can triggered, the positive
371 feedback between the climate and melt ponds will drive the climate to a warm state and
372 further increasing σ is not useful. Therefore, moderate temperature fluctuation of ±1.5 °C
373 (3σ where σ = 0.5 °C) within a large grid cell is enough to trigger prevalent formation of
374 melt ponds and snowball Earth deglaciation (see discussion below) when $p\mathrm{CO}_2$ is 0.1 bar.

375 In formulating the melt pond model, we also assumed that the temperature profile of pond
376 water is linear (Fig. 2). Since this temperature gradient of water determines the downward
377 growth of pond water (equ. (3)), it is necessary to test how sensitive the result is to this

temperature gradient. The results show similar bifurcation behavior as those for the tests of σ (Fig. 10), i.e. as long as the gradient is 0.75 times or larger than that implied by the linear temperature profile, melt ponds will develop significantly and deglaciation will start.

4.2 Availability of dust

Results in section 3.3 indicate that the dust effect on snow aging cannot be much weaker than that in present day in order for the effect of melt ponds to kick in. Using a one-dimensional model, (Abbot & Halevy, 2010) estimated that dust could be abundant in the atmosphere due to weak hydrological cycle in a snowball Earth. In their estimate, dust sources were limited to unglaciated land. An additional source could be the dust locked in the thick sea ice during long snowball Earth period and transported to the net sublimation region of low latitude (Hoffman et al., 2017a; Li & Pierrehumbert, 2011a). Moreover, because snow precipitation rate is small during a snowball Earth, little dust may be needed to mix with surface snow in order for it to age. Therefore, we may expect that snow aging near the end of a snowball Earth event was as effective in reducing snow albedo as in present day even though atmospheric dust loading might be lower.

4.3 Difference in results between implicit and explicit melt ponds

In the implicit melt pond formulation, surface temperature can be used as a surrogate for appearance of melt ponds. Taking the experiment IMP80 as an example, narrow belt of melt water appears seasonally between 23°N-33°N and 22°S-60°S (Fig. 11a,b) at model year 25. These belts of melt water expands substantially at equilibrium and the maximum monthly mean temperature can be as high as 8 °C (Fig. 11c,d). At such high monthly

400 temperature, it may be expected that deep melt ponds form and sustain through the year.
401 However, they always disappear completely during winter under such formulation.
402 Moreover, it is suspicious that subtropical temperature can reach this high (compared to
403 the temperature at equator); the too easy formation of melt ponds and strong positive
404 feedback between melt-pond albedo and temperature may have induced this surprisingly
405 high monthly temperature.

406 In this formulation, melt-pond albedo does not decrease once the surface temperature is
407 higher than 0 °C (Fig. 3). Otherwise, the temperature in these two regions can be even
408 higher and it might give you the illusion that deglaciation of snowball Earth will start
409 from these regions. There is no permanent melt ponds appearing at equator, as can be
410 inferred from Fig. 11c,d. Therefore, it is hard to know where the deglaciation will start
411 even when a formulation for implicit melt pond is included in the model. If a more
412 aggressive formulation is used, e.g. experiment IMP60, permanent melt pond appears
413 near the equator (not shown), but the maximum monthly temperature in the subtropical
414 regions can reach 12 °C, which again suggest heavy melting and probable deglaciation
415 there.

416 Inclusion of explicit formulation of melt ponds in the model removes the ambiguity
417 above. Although melt ponds first appear seasonally in the mid latitude region during the
418 run (Fig. 12a,b), permanent deep melt ponds appear only within a wide belt (±20° latitude)
419 around the equator at equilibrium (Fig. 12c,d). The results also tell us that the maximum
420 monthly surface temperature at mid latitude can reach ~15 °C (Fig. 13c) without forming
421 permanent melt ponds, because the minimum monthly temperature at the same location
422 can be as low as -40 °C (Fig. 13).

The depth of water at equator reaches 10 m at model year 200 and continues to grow with time (not shown). It demonstrates that at the end of a snowball Earth, large swamps of water appears over more than half of the globe at all seasons, but deep perennial water accumulates only at the equator. Eventually, such deep water should become thick enough to break the ice sheet and start the deglaciation, see more discussion below.

4.4 Deglaciation of a snowball Earth

The dynamics of thick sea ice over oceans during a snowball Earth is very similar to the ice shelves around Antarctica. The largest difference between them maybe that the ice sheet in the former is restricted in all directions since there is no open ocean, while the ice shelves in the latter can move freely towards the ocean in some direction. Nevertheless, the disintegration of the ice shelves may provide some clue for how the snowball Earth starts to deglaciate. Many of the disintegration events around Antarctica had been observed and the mechanisms studied (Scambos et al., 2009; Scambos et al., 2000). Among these events, the most significant one may be the disintegration of the Larsen B ice shelf, approximately 3250 km^2 collapsed in just a few days in March 2002 (Shepherd et al., 2003).

For all the disintegration events around Antarctica, melt ponds or lakes formed by meltwater were observed prior to the disintegration. If fractures or crevasses exist on the ice surface, meltwater infilling will increase the tensile stress at the bottom tip of the fractures. If the tensile stress is greater than the fracture toughness of the ice, the fractures will then propagate downward and cut through the whole ice sheet. For this to happen,

445 the initial fracture needs to be deep enough and the meltwater supply should be sufficient.
446 Once it happens, it progresses quickly, normally within one melt season. The critical
447 initial fracture depth was estimated for the Larsen B ice shelve to be 24-30 m if the upper
448 limit for the fracture toughness (400 kPa $m^{1/2}$) is used (Scambos et al., 2000). Fractures or
449 crevasses can form near the grounding line where the continental ice sheets become afloat,
450 and be advected away from the coastal region (Scambos et al., 2000). Therefore, we may
451 expect that some crevasses exist, even in a snowball Earth.

452 If there are no pre-existing fractures, the meltwater, if deep enough, can induce cracking
453 of ice by itself (Banwell et al., 2013). The meltwater normally gathers into discrete lakes
454 on the ice surface. The lakes depress the ice sheet and rings of forebulges form around the
455 lakes, where the tensile stress may be large enough to create fractures at the surface. For
456 an ice shelf of 200 m thick, the depth of lakes needs to be a few meters deep (Banwell et
457 al., 2013). The ice thickness in a snowball Earth is between 500 – 700 m near the equator
458 when $p\mathrm{CO_2}$ is 0.1 bar (Abbot et al., 2013a), the required water depth may thus be greater.
459 This should not be a problem since the melt season of the equatorial region is all year
460 long. The subtropical region, however, may not have a long enough melt season to induce
461 cracks on the ice sheet. Moreover, the general slope of the ice surface is downward from
462 pole to equator (Li & Pierrehumbert, 2011a) so the melt water produced in the subtropical
463 region may flow towards the equator. This flow is not simulated in the current work.

464 Once the ice sheet is cut through by the cracks, the meltwater on the surface will drain
465 into the oceans beneath. The drainage of one lake induces a train of drainage events
466 around itself. The drainage events induce more cracking of the ice sheet from the bottom
467 (Banwell et al., 2013). With ample meltwater supply, the belt of ice sheet around the

equator will eventually be cut into pieces. The surface melting and the drainage of meltwater may continuously shrink the ice blocks there and create an area of open ocean. At the very least, equatorial melt water can grow continuously at the expense of the ice below; the equatorial ice sheet will be just melt away if breaking does not happen. We think this marks the start of the snowball Earth deglaciation. Our simulations above show that 0.1 bar of CO_2 is enough to trigger the deglaciation of snowball Earth while 0.09 bar is not (not shown).

5. Conclusions

The deglaciation of a snowball Earth is studied by explicitly simulating the formation of melt ponds on thick sea-ice sheet. Without considering melt ponds, snowball Earth cannot start to deglaciate when pCO_2 reaches 0.1 bar even if the effect of snow aging is considered; the annual mean equatorial surface temperature is only approximately -7.7 °C. The formation of melt ponds provides a strong positive feedback and the equilibrium equatorial temperature is increased to substantially 6.1 °C, indicating that previous studies not considering melt ponds could have significantly overestimated the threshold pCO_2 for snowball Earth deglaciation. More importantly, the results clearly demonstrate for the first time that although seasonal melt water appears first in the subtropical region, perennial melt water only appears near the equator. Deep ponds of melt water will form approximately ±15° within the equator. Their depth continues to grow and is expected to eventually break up the thick ice sheet there. This removes the ambiguity in judging the start of snowball Earth deglaciation by temperature or implicit melt ponds.

Acknowledgement

The simulations were done on the High-performance Computing Platform of Peking University. Y. Liu is supported by the National Natural Science Foundation of China under grant 41875090 and 41761144072. The model results that support the findings of this study are available on Zenodo with the identifier http://doi.org/10.5281/zenodo.4013203.

Reference

Abbot, D. S., and I. Halevy (2010), Dust Aerosol Important for Snowball Earth Deglaciation, *J Climate*, *23*(15), 4121-4132, doi:10.1175/2010jcli3378.1.

Abbot, D. S., and R. T. Pierrehumbert (2010), Mudball: Surface dust and Snowball Earth deglaciation, *J Geophys Res-Atmos*, *115*, doi:10.1029/2009jd012007.

Abbot, D. S., A. Voigt, D. Li, G. L. Hir, R. T. Pierrehumbert, M. Branson, D. Pollard, and D. D. B. Koll (2013a), Robust elements of Snowball Earth atmospheric circulation and oases for life, *Journal of Geophysical Research: Atmospheres*, *118*(12), 6017-6027, doi:10.1002/jgrd.50540.

Abbot, D. S., A. Voigt, D. W. Li, G. Le Hir, R. T. Pierrehumbert, M. Branson, D. Pollard, and D. D. B. Koll (2013b), Robust elements of Snowball Earth atmospheric circulation and oases for life, *J Geophys Res-Atmos*, *118*(12), 6017-6027.

Ashkenazy, Y., H. Gildor, M. Losch, and E. Tziperman (2014), Ocean circulation under globally glaciated Snowball Earth conditions: Steady-state solutions, *Journal of physical oceanography*, *44*(1), 24-43.

Axenrot, T., M. Ogonowski, A. Sandström, and T. Didrikas (2009), Multifrequency discrimination of fish and mysids, *ICES Journal of Marine Science*, *66*(6), 1106-1110.

Banwell, A. F., D. R. MacAyeal, and O. V. Sergienko (2013), Breakup of the Larsen B Ice Shelf triggered by chain reaction drainage of supraglacial lakes, *Geophysical Research Letters*, *40*(22), 5872-5876.

Bogorodsky, P., A. Marchenko, and A. Pnyushkov (2006), Thermodynamics of freezing melt ponds, paper presented at 18th IAHR International Symposium on Ice, Sapporo, Japan.

Briegleb, B., C. Bitz, E. Hunke, W. Lipscomb, M. Holland, J. Schramm, Moritz, and RE (2004), Scientific description of the sea ice component in the Community Climate System Model, *Version*, *3*, 70.

Caldeira, K., and J. F. Kasting (1992), Susceptibility of the early Earth to irreversible glaciation caused by carbon dioxide clouds, *Nature*, *359*(6392), 226-228, doi:10.1038/359226a0.

524 Collins, W. D., et al. (2004), Description of the NCAR Community Atmosphere Model
525 (CAM 3.0), *NCAR TECHNICAL NOTES*, *NCAR/TN–464+STR*, 226.

526 Eicken, H., H. R. Krouse, D. Kadko, and D. K. Perovich (2002), Tracer studies of
527 pathways and rates of meltwater transport through Arctic summer sea ice, *Journal*
528 *of Geophysical Research - Oceans*, *107*(C10), 8046-SHE 8022-8020,
529 doi:10.1029/2000JC000583.

530 Hoffman, P. F., D. S. Abbot, Y. Ashkenazy, D. I. Benn, J. J. Brocks, P. A. Cohen, G. M. Cox,
531 J. R. Creveling, Y. Donnadieu, and D. H. Erwin (2017a), Snowball Earth climate
532 dynamics and Cryogenian geology-geobiology, *Science Advances*, *3*(11), e1600983.

533 Hoffman, P. F., et al. (2017b), Snowball Earth climate dynamics and Cryogenian
534 geology-geobiology, *Science Advances*, *3*(11).

535 Hoffman, P. F., A. J. Kaufman, G. P. Halverson, and D. P. Schrag (1998), A
536 Neoproterozoic snowball earth, *Science*, *281*(5381), 1342-1346.

537 Hu, Y., J. Yang, F. Ding, and W. R. Peltier (2011), Model-dependence of the CO2
538 threshold for melting the hard Snowball Earth, *Clim Past*, *7*(1), 17-25,
539 doi:10.5194/Cp-7-17-2011.

540 Hunke, E. C., W. H. Lipscomb, A. K. Turner, N. Jeffery, and S. Elliott (2013), CICE: the
541 Los Alamos Sea Ice Model Documentation and Software User's Manual Version 5.0
542 LA-CC-06-012.

543 Le Hir, G., Y. Donnadieu, G. Krinner, and G. Ramstein (2010), Toward the snowball
544 earth deglaciation... *Clim Dynam*, *35*(2-3), 285-297, doi:10.1007/S00382-010-0748-
545 8.

546 Le Hir, G., G. Ramstein, Y. Donnadieu, and R. T. Pierrehumbert (2007), Investigating
547 plausible mechanisms to trigger a deglaciation from a hard snowball Earth, *Cr Geosci*,
548 *339*(3-4), 274-287.

549 Li, D., and R. T. Pierrehumbert (2011a), Sea glacier flow and dust transport on
550 Snowball Earth, *Geophysical Research Letters*, *38*(17).

551 Li, D. W., and R. T. Pierrehumbert (2011b), Sea glacier flow and dust transport on
552 Snowball Earth, *Geophys Res Lett*, *38*.

553 Liu, Y., J. Yang, H. Bao, B. Shen, and Y. Hu (2020), Large equatorial seasonal cycle
554 during Marinoan snowball Earth, *Science Advances*, *6*(23), eaay2471.

555 Oleson, K. W., et al. (2004), Technical description of the Community Land Model
556 (CLM), *NCAR Technical Note*, *NCAR/TN-495+STR*, 174, doi:10.5065/D6N877R0.

557 Paterson, W. S. B. (1994), *Physics of glaciers*, Butterworth-Heinemann.

558 Petrich, C., H. Eicken, C. M. Polashenski, M. Sturm, J. P. Harbeck, D. K. Perovich, and D.
559 C. Finnegan (2012), Snow dunes: A controlling factor of melt pond distribution on
560 Arctic sea ice, *Journal of Geophysical Research: Oceans*, *117*(C9).

561 Pierrehumbert, R. T. (2004), High levels of atmospheric carbon dioxide necessary
562 for the termination of global glaciation, *Nature*, *429*(6992), 646-649,
563 doi:10.1038/nature02640.

564 Polashenski, C., D. Perovich, and Z. Courville (2012), The mechanisms of sea ice melt
565 pond formation and evolution, *J Geophys Res-Oceans*, *117*.

566 Richter-Menge, J. A., D. K. Perovich, and W. S. Pegau (2001), Summer ice dynamics
567 during SHEBA and its effect on the ocean heat content, *Annals of glaciology*, *33*(1),
568 201-206, doi:10.3189/172756401781818176.

569 Roeckner, E., T. Mauritsen, M. Esch, and R. Brokopf (2012), Impact of melt ponds on
570 Arctic sea ice in past and future climates as simulated by MPI-ESM, *Journal of*
571 *Advances in Modeling Earth Systems*, *4*(3).

572 Ross, S. M. (2010), *A First Course in Probability*, Pearson Prentice Hall.

573 Scambos, T., H. A. Fricker, C.-C. Liu, J. Bohlander, J. Fastook, A. Sargent, R. Massom,
574 and A.-M. Wu (2009), Ice shelf disintegration by plate bending and hydro-fracture:
575 Satellite observations and model results of the 2008 Wilkins ice shelf break-ups,
576 *Earth and Planetary Science Letters*, *280*(1-4), 51-60.

577 Scambos, T. A., C. Hulbe, M. Fahnestock, and J. Bohlander (2000), The link between
578 climate warming and break-up of ice shelves in the Antarctic Peninsula, *Journal of*
579 *Glaciology*, *46*(154), 516-530.

580 Scharien, R., K. Hochheim, J. Landy, and D. Barber (2014), Sea ice melt pond fraction
581 estimation from dual-polarisation C-band SAR-Part 2: Scaling in situ to Radarsat-2,
582 *TCD*, *8*(1), 845-885.

583 Schwarz, G., W. Frenzel, W. M. Richter, L. Täuscher, and G. Kubsch (2016), A
584 multidisciplinary science summer camp for students with emphasis on
585 environmental and analytical chemistry, *Journal of Chemical Education*, *93*(4), 626-
586 632.

587 Shepherd, A., D. Wingham, T. Payne, and P. Skvarca (2003), Larsen ice shelf has
588 progressively thinned, *Science*, *302*(5646), 856-859.

589 Stepanenko, V. M., S. Goyette, A. Martynov, M. Perroud, X. Fang, and D. Mironov
590 (2010), First steps of a Lake Model intercomparison project: LakeMIP.

591 Tajika, E. (2003), Faint young Sun and the carbon cycle: implication for the
592 Proterozoic global glaciations, *Earth and Planetary Science Letters*, *214*(3-4), 443-
593 453.

594 Taylor, P., and D. Feltham (2004), A model of melt pond evolution on sea ice, *Journal*
595 *of Geophysical Research: Oceans*, *109*(C12).

596 Webster, M., S. Gerland, M. Holland, E. Hunke, R. Kwok, O. Lecomte, R. Massom, D.
597 Perovich, and M. Sturm (2018), Snow in the changing sea-ice systems, *Nature*
598 *Climate Change*, *8*(11), 946-953.

599

600

Table. 1 Summary of experiments and main results.

Experiment	Snow aging parameter r_d	6°S~6°N Temperature (°C)	Global Temperature(°C)	Start year of deglaciation	Surface Albedo
Default	0.3*	-29.1	-51.0	-	0.74
rd1	0.3	-7.7	-19.9	-	0.61
rd2	0.2	-7.9	-20.1	-	0.61
rd3	0.1	-9.1	-21.1	-	0.62
rd4	0.03	-9.7	-21.8	-	0.62
IMP80	0.3	-0.4	-13.7	-	0.53
IMP60	0.3	2.7	-9.9	15	0.46
EMP_rd1	0.3	6.1	-6.9	40	0.38
EMP_rd2	0.2	6.1	-7.0	65	0.39
EMP_rd3	0.1	-7.7	-18.3	-	0.59
EMP_rd4	0.03	-7.8	-18.6	-	0.59

*** snow age is fixed to 0 for snow that is deeper than 800 mm water equivalent.**

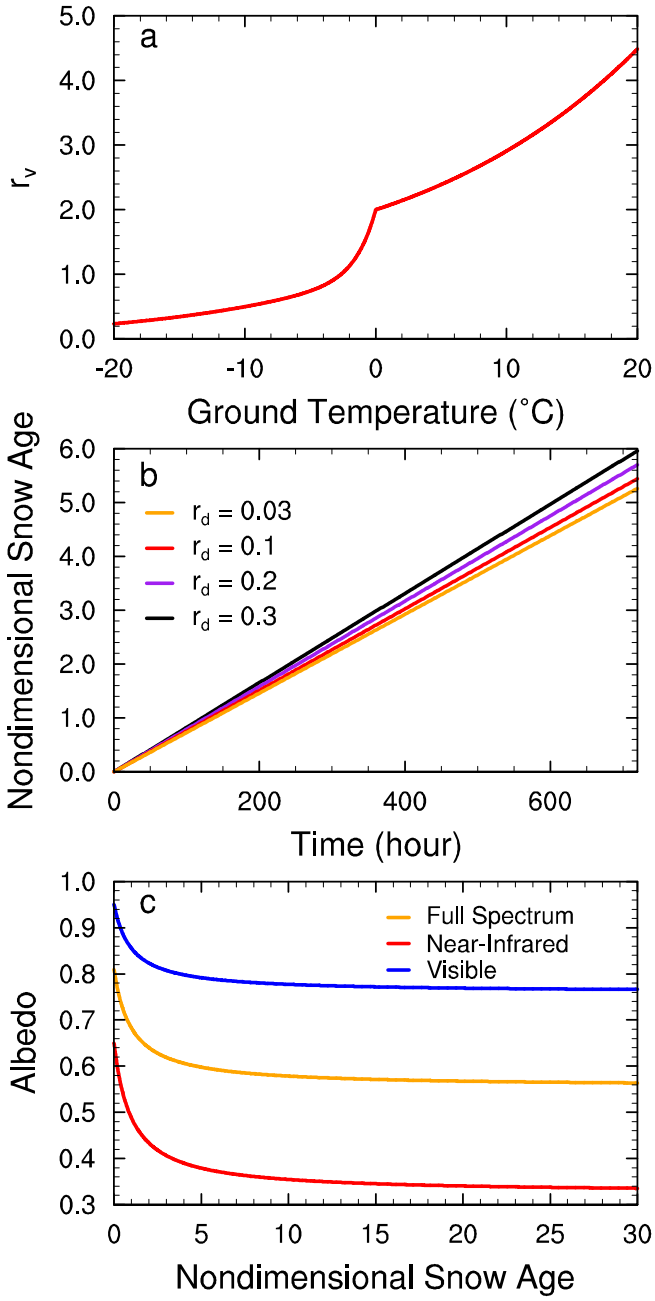

604

605 **Fig. 1** Snow aging and its albedo effect. a) change of snow-aging parameter r_v with

606 temperature; b) growth of non-dimensional snow age with time for different r_d when

607 temperature is fixed at 0 °C and without the change in mass of snow water; c) change of

608 snow albedo with snow age.

609

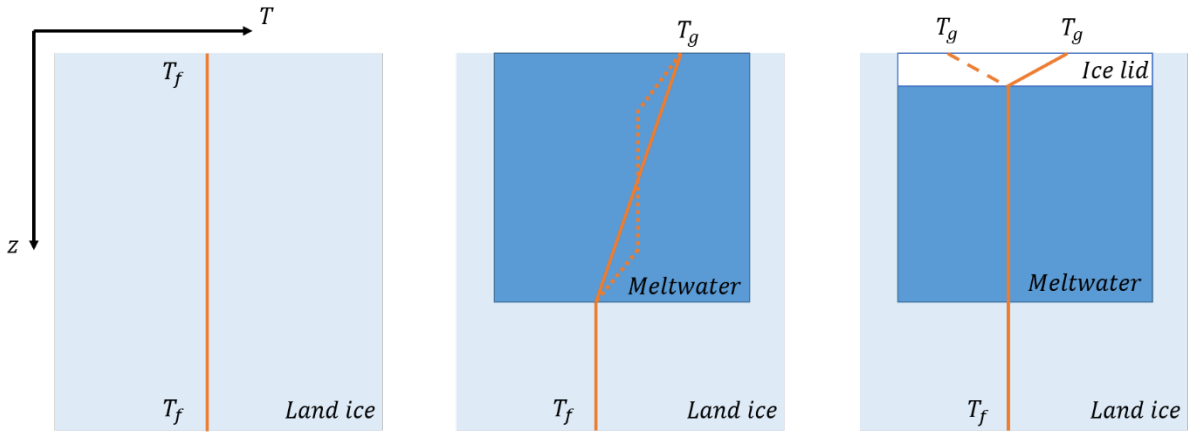

Fig. 2 Melt ponds at different stages. The orange lines represent the vertical temperature profiles assumed in our melt pond formulation. T_f is the freezing temperature of pure ice, and T_g is the temperature at ground surface. The dotted line in stage II represents possible temperature profile when T_g is around 4 °C.

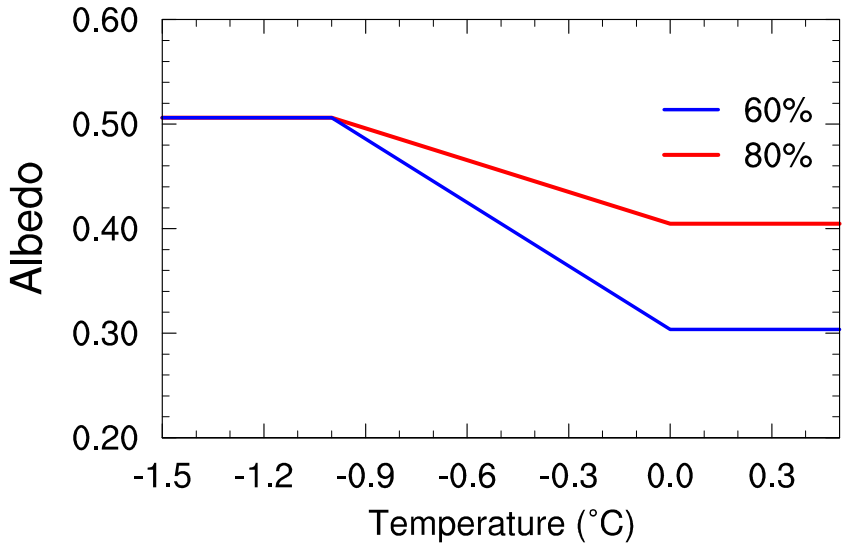

Fig. 3 The linear dependence of surface albedo of ice on temperature in the implicit formulation of melt ponds.

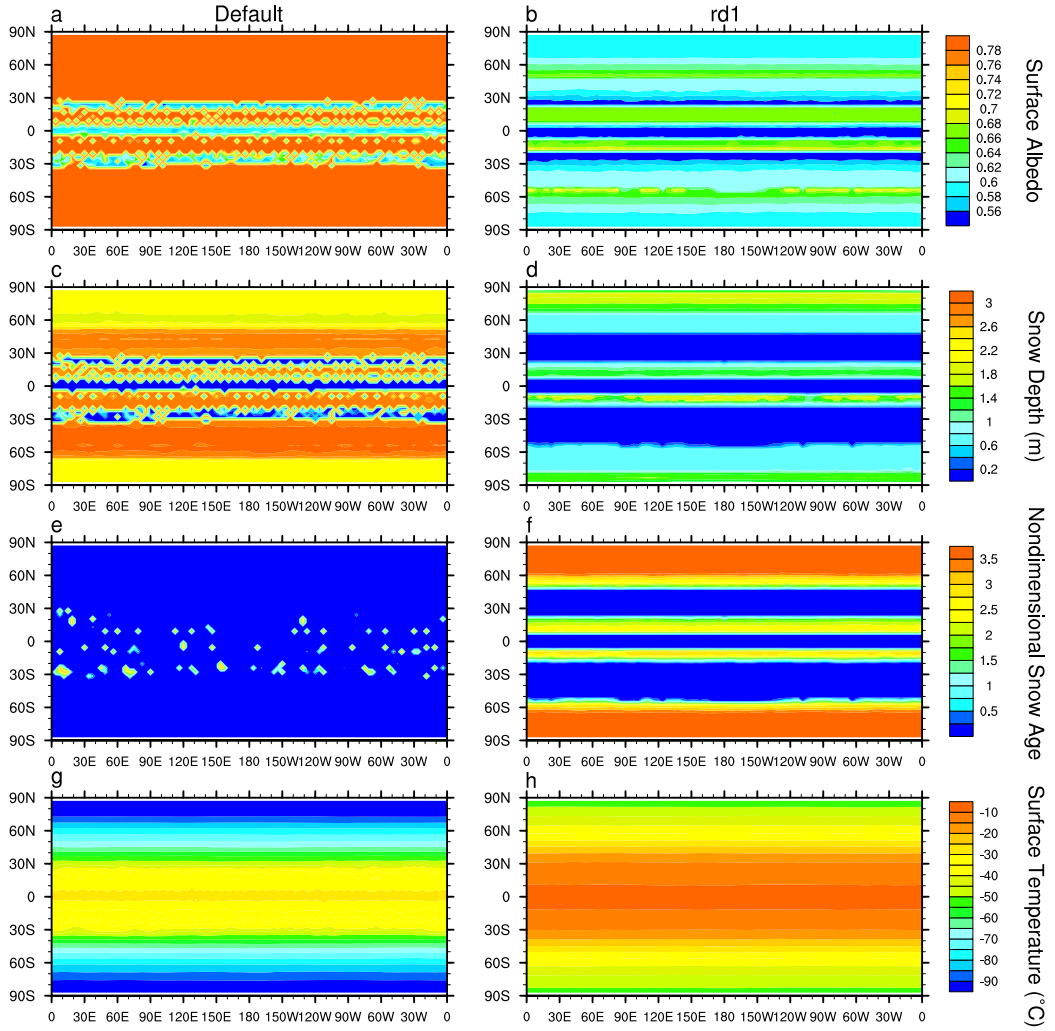

627
628 **Fig. 4** Annual-mean surface albedo (a, b), snow depth (c, d), nondimensional snow age (e,
629 f) and surface temperature (g, h) at equilibrium state. Panels on the left and right are for
630 experiments Default and rd1, respectively. Note that the deep blue in e) indicates thick
631 (>800 mm water equivalent) snow while in f) it indicates thin (a few 10s of mm) new
632 snow.
633

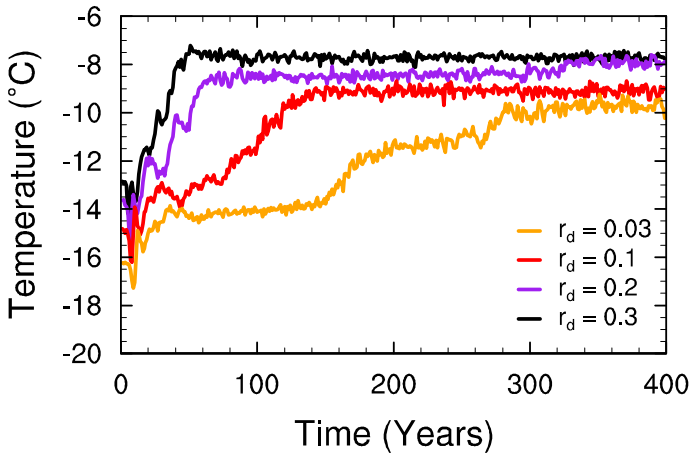

634

635 Fig. 5 Time series of annual mean equatorial (6°S – 6°N) surface temperature for

636 experiments rd1 to rd4.

637

638

639

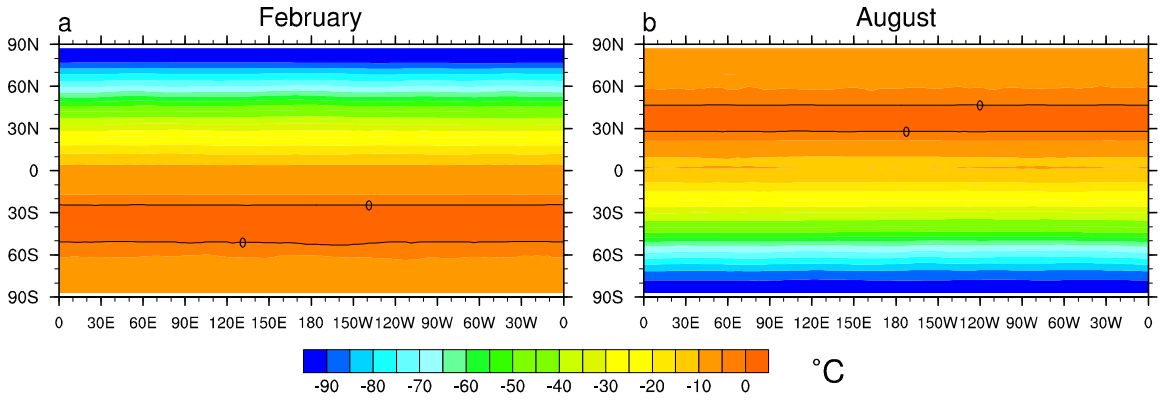

Fig. 6 Monthly mean surface temperature for February and August in experiment rd1 at equilibrium.

644

645

646

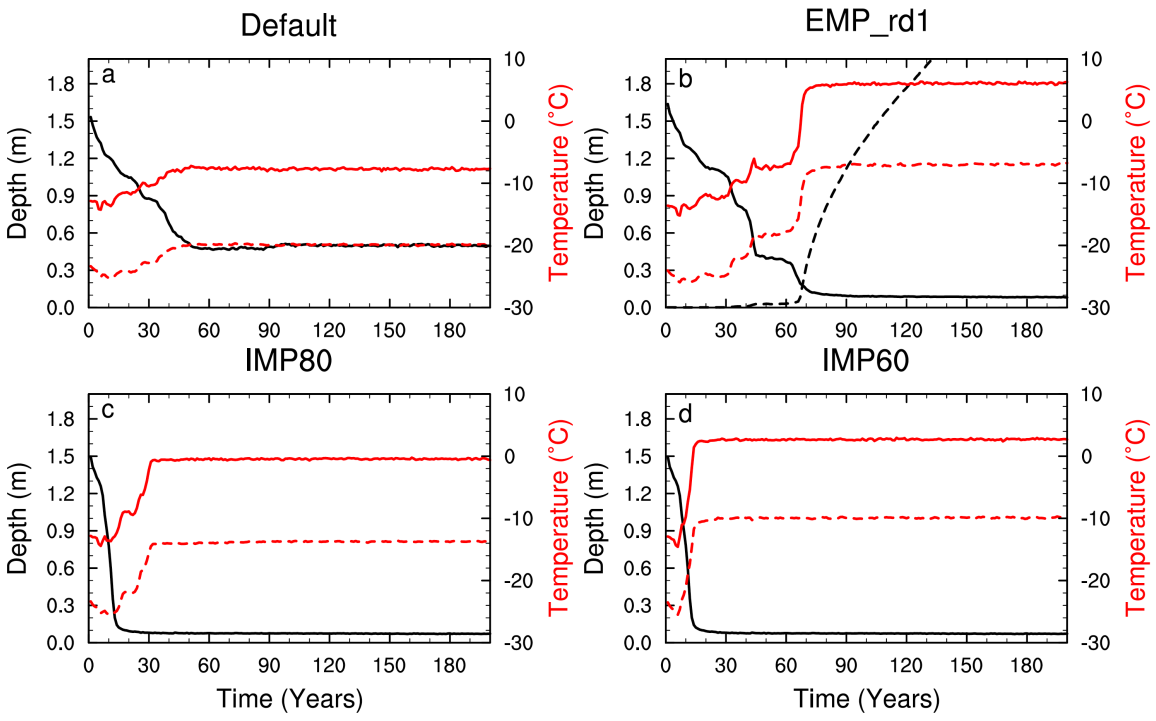

647

648 **Fig. 7** Annual-mean equatorial (6°S~6°N) mean surface temperature (red solid curve),

649 global mean surface temperature (red dash curve) and global mean snow depth (blue solid

650 curve) for the a) Default b) EMP_rd1 c) IMP80 d) IMP60. Black dashed cure in b)

651 represents global mean thickness of melt water.

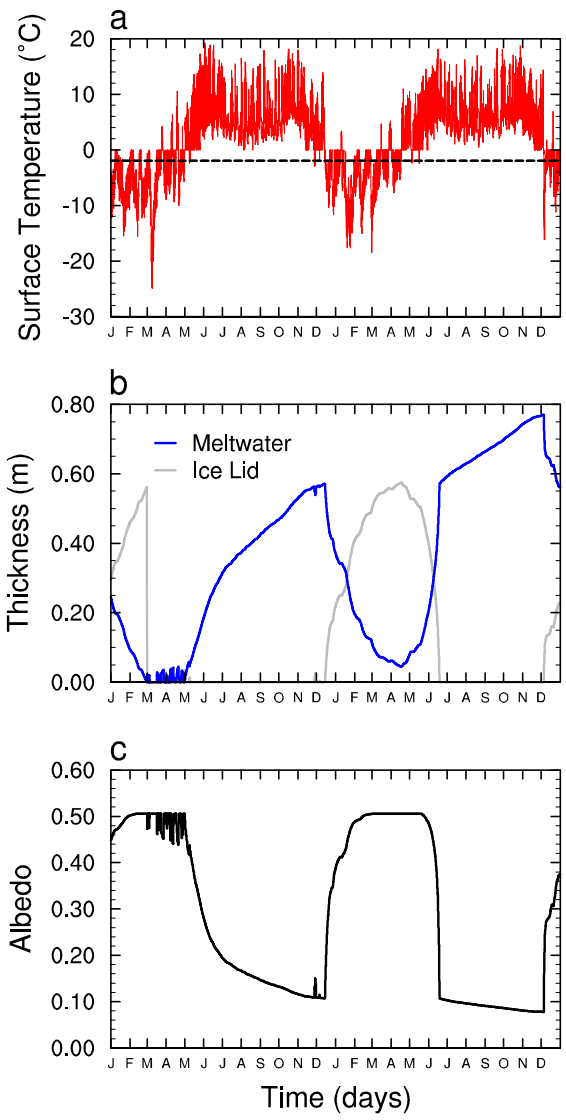

652 **Fig. 8** Time series of daily a) surface temperature, b) thickness of meltwater and ice lid,
653 and c) albedo from model year 40 to 41 at a point located at (180°E, 16.7°N) in
654 experiment EMP_rd1. The black dashed line in a) indicates the temperature -2σ (where σ
655 = 1 °C) above which the formation of melt pond is possible.

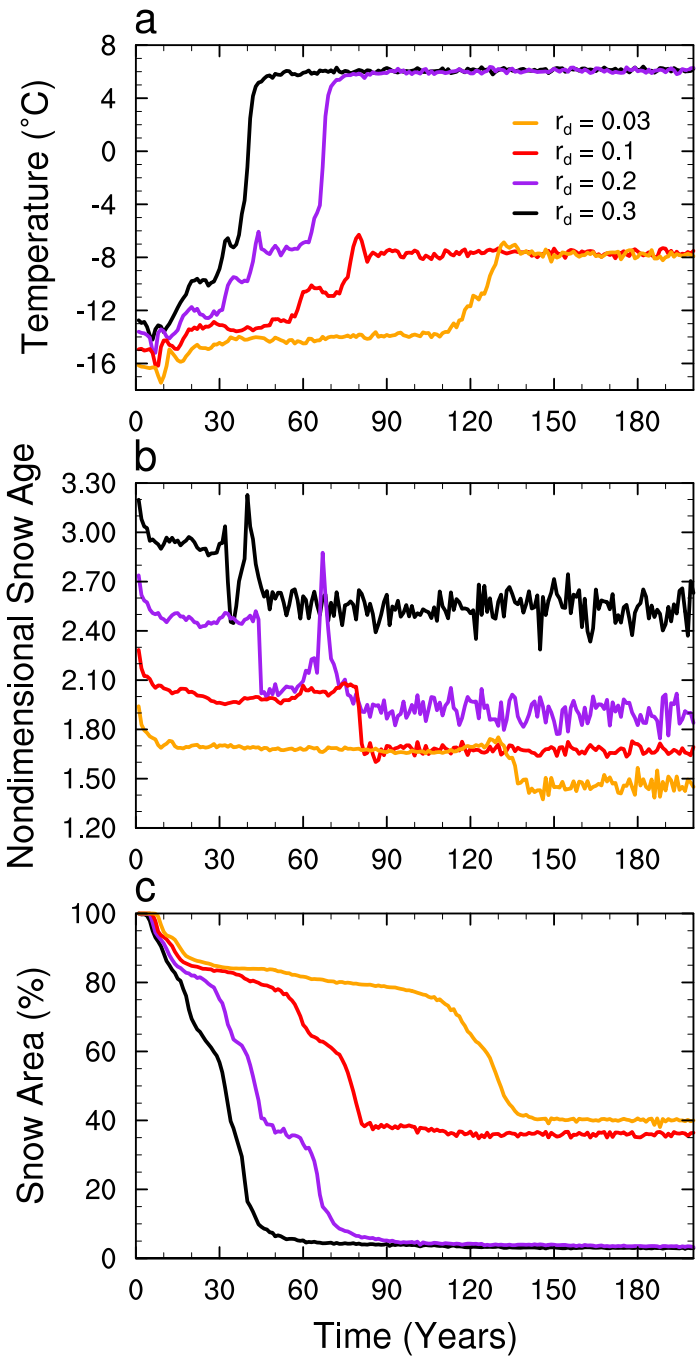

656

657 **Fig. 9** Time series of annual-mean of a) equatorial (6°S~6°N) surface temperature, b)

658 global mean non-dimensonal snow age and c) snow area (both averaged over area only

659 where snow depth is greater than 0.3 m) for experiments EMP_rd1, to EMP_rd4.

660

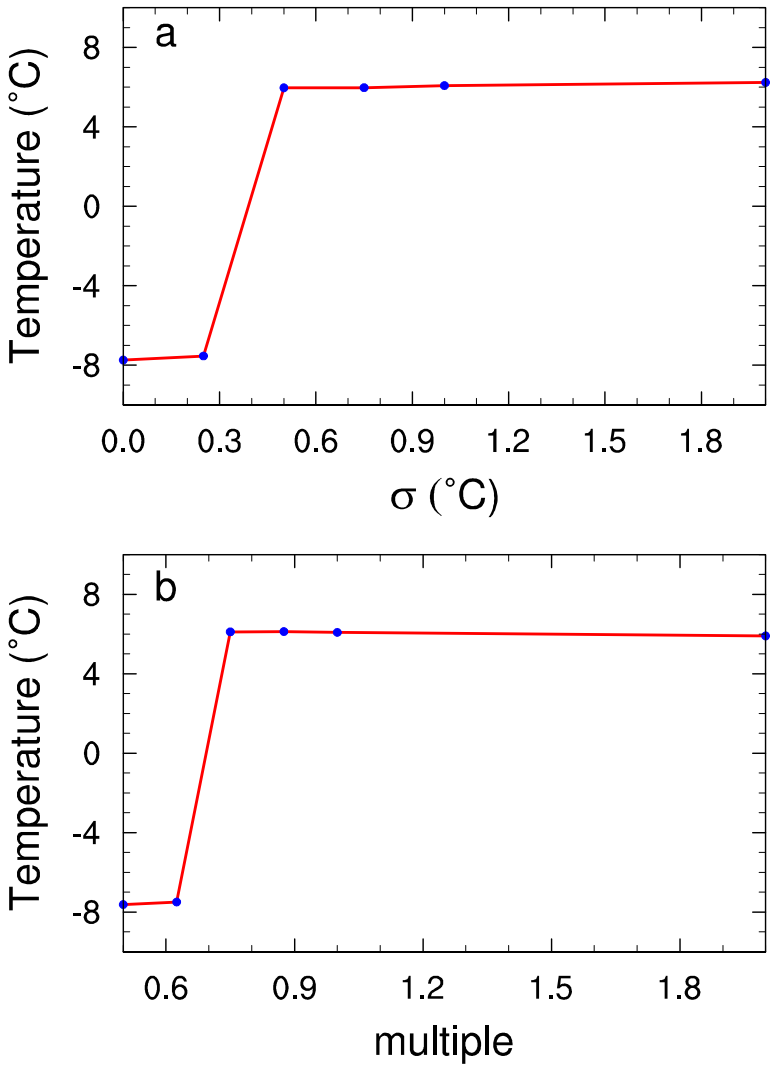

661

662 **Fig. 10** Sensitivity of equilibrium annual mean equatorial (6°S – 6°N) surface

663 temperature to a) σ in equ. (7) and b) temperature gradient in equ. (3). The experimental

664 setup is the same as EMP_rd1.

665

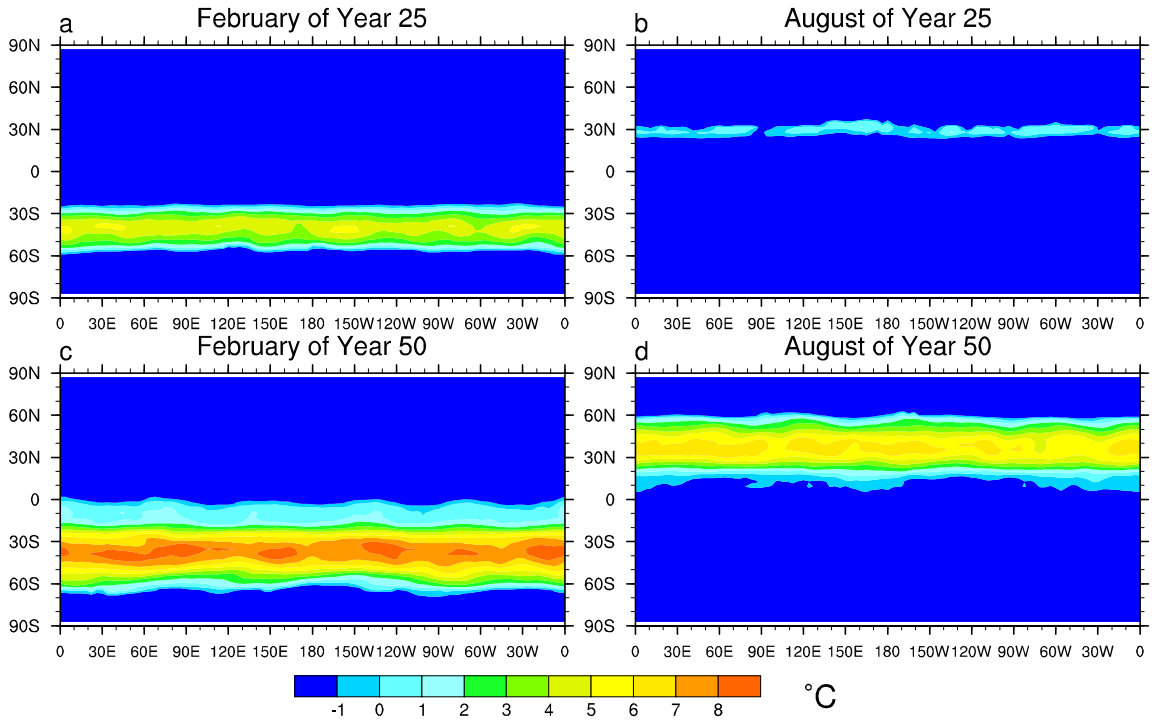

667 **Fig. 11** Distribution of temperature as a surrogate for implicit melt ponds in experiment
668 IMP80. All regions with temperature greater than -1 °C (colors excluding the deep blue)
669 can be approximately considered as having melt ponds.

670

671

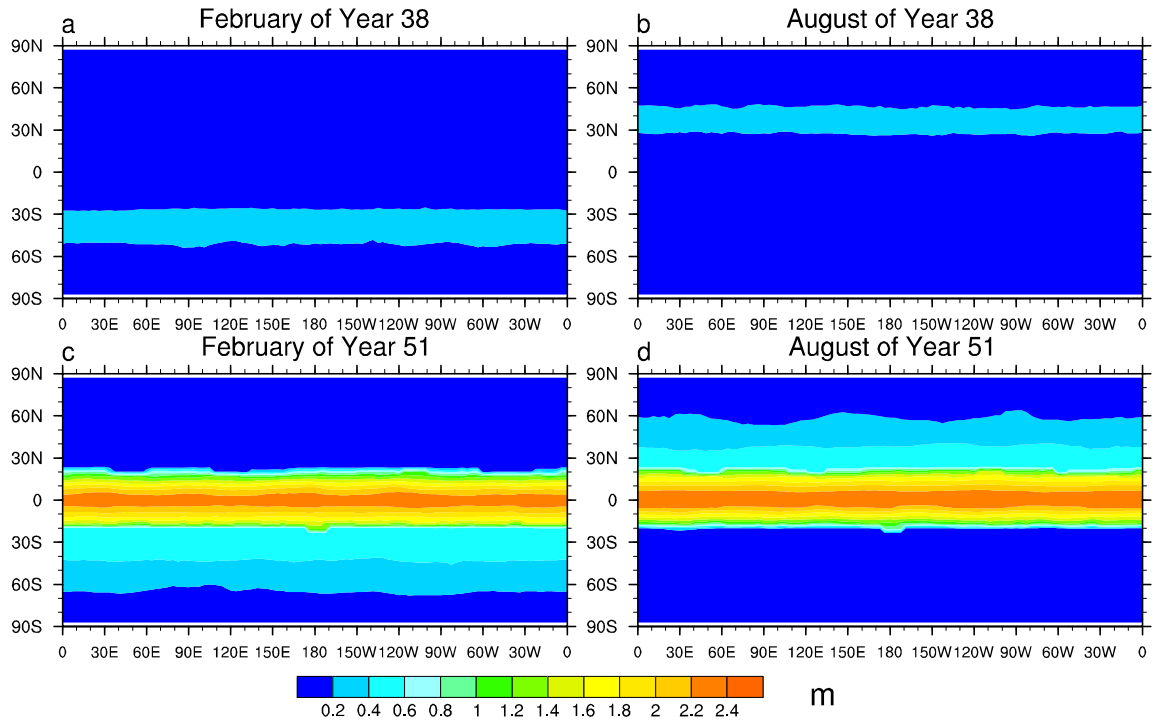

672

673 **Fig. 12** Distribution of thickness of meltwater in February and August in experiment

674 EMP_rd1. a) and b) are for model year 38, c) and d) are for model year 51.

675

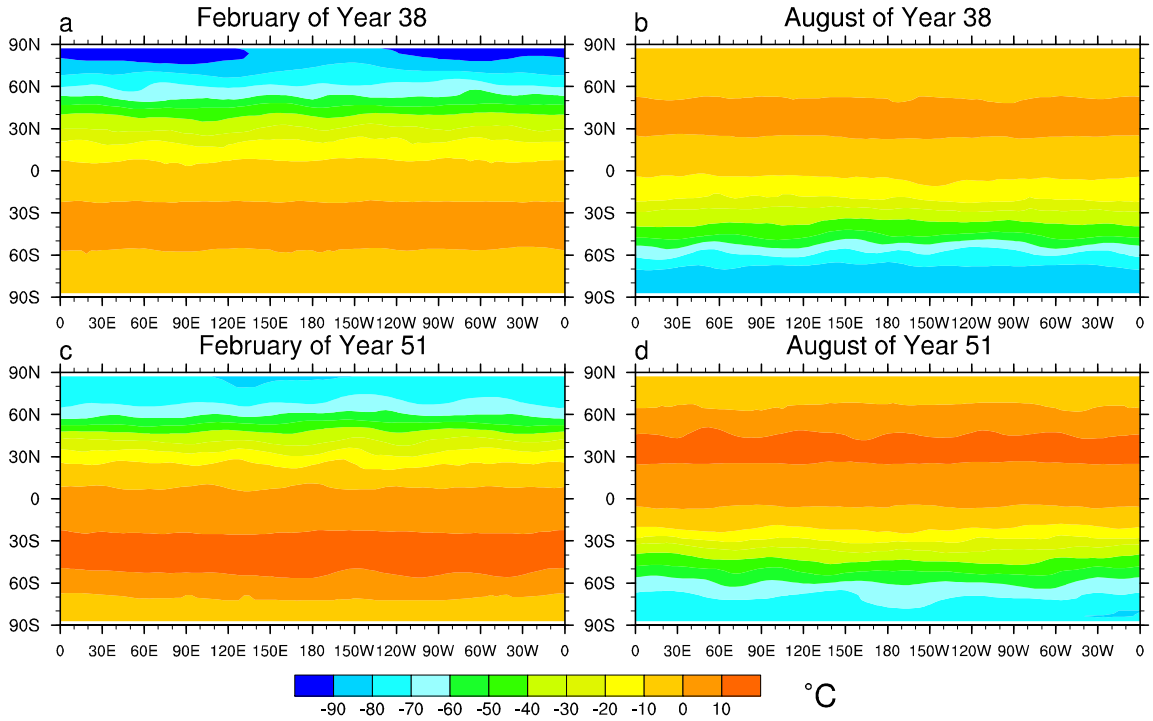

Fig. 13 Similar to Fig. 12 except here the surface temperature is shown.